ЖЭТФ, 2008, том 133, вып. 4, стр. 770–780 

# PHOTOREFRACTIVE DECELERATION OF LIGHT PULSES

***B. Sturman*** [a]*, ***E. Podivilov*** [a], ***M. Gorkunov*** [b]

[a] *Institute of Automation and Electrometry, Russian Academy of Sciences*
*630090, Novosibirsk, Russia*

[b] *Institute of Crystallography, Russian Academy of Sciences*
*119333, Moscow, Russia*

Received August 28, 2007

We theoretically study the effect of light deceleration in photorefractive nonlinear media. This includes consideration of different types of the photorefractive nonlinear response, different wave interaction schemes, and an analysis of the influence of the input parameters, such as the input temporal pulse width and the coupling strength, on the output pulse characteristics: the time delay, the propagation velocity, the amplification factor, and the output width. We show that the photorefractive light deceleration has numerous advantages over the other known techniques. It works already at low intensities, at room temperature, and within wide spectral ranges and offers a vast variety of handles for manipulating light pulses. An analogy with the light deceleration method based on the quantum effect of electromagnetically induced transparency in ultra-cold resonant gases is also considered.

PACS: 42.65.Hw, 42.50.Gy, 78.20.Bh

## 1. INTRODUCTION

The effect of deceleration of light pulses has attracted a great research interest during the last years (see, e.g., reviews [1–5] and the references therein). The most impressive results on the light deceleration are usually attributed to the quantum effect of electromagnetically induced transparency (EIT) [6], which implies the use of narrow atomic resonances, low temperatures, and high light intensities. In particular, deceleration of light pulses down to 17 m/s was achieved with Bose–Einstein-condensed ultra-cold gases [2]. The EIT-based techniques also allow the so-called complete stop and storage of light pulses with their possible release on demand [7]. Attempts to use room-temperature resonances in solids for light deceleration are known as well [8–10]. The achieved deceleration characteristics are still modest and high pump intensities are required.

A clear concern about incorrect usage of physical terms in the literature on light deceleration has also been expressed [11]. It reflects the fact that the actual characteristics of nonlinear pulse propagation are often mixed with the terms of linear optics, like the group velocity and dispersion. The linear and nonlinear methods for light deceleration must indeed be clearly distinguished. In particular, the achieved ultra-low light velocities are fully due to nonlinear effects.

Apart from an obvious fundamental interest, the nonlinear light deceleration is promising for development of sensitive detectors and delay lines [5, 12] and, potentially, for quantum information processing [13]. For practical purposes, the use of ambient temperatures, solid-state materials, and common light sources has actually no real alternative.

Recently, it has been demonstrated theoretically and experimentally in some special cases that the deceleration of light pulses can be implemented with the use of the photorefractive (PR) nonlinearity [14, 15]. The pulse propagation velocities lower than 0.025 cm/s were achieved. Similar attempts to employ the PR nonlinearity were also made in [16, 17].

In this paper, we theoretically study the potential of the strong PR nonlinearity (see, e.g., [18, 19]) for deceleration of light pulses. This includes analysis of the main output characteristics, such as the shape, the delay time, the output width, and the amplification factor, versus the input parameters — the input width, the coupling strength, and the pump intensity — for

*E-mail: sturman@iae.nsk.su

different types of the PR response and different interaction schemes. We also analyze the conditions for strong deceleration of light pulses with minimum possible distortions; this leads us to the range of large coupling strengths and, correspondingly, of strongly nonlinear effects.

General advantages and distinctive features of the proposed PR method of light deceleration are worth mentioning. In contrast to other techniques, no frequency adjustment is needed; broad absorption spectra in the visible and near infra-red range are available. Operation at room temperature and intensities of continuous-wave lasers, $10^{-2}$–$10^{3}$ W/cm$^2$, is ensured. Because the PR nonlinearity is caused by light-induced electric fields, the wealth of charge-transport mechanisms in photosensitive materials allows shaping the spectral characteristics of the nonlinear response. Achievement of large values of the coupling strength does not present serious difficulties.

Despite numerous special features, the PR method offers surprizing analogies with the EIT-based deceleration technique. These analogies also belong to the subject of this paper.

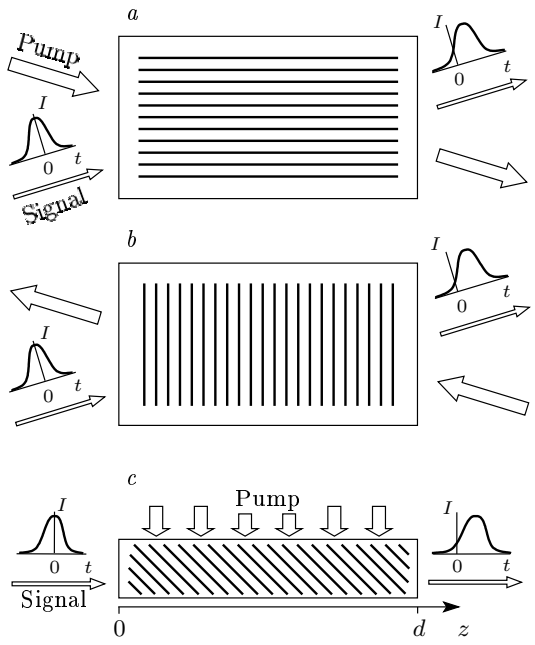


**Fig. 1.** Three main geometries, transmission ($a$), reflection ($b$), and 90-degree ($c$), for deceleration of light pulses. The parallel dashes represent the grating fringes. The propagation distance for the signal wave is $d$

## 2. GENERAL RELATIONS

In what follows, we restrict ourselves to the two-wave coupling schemes (interaction geometries) depicted in Fig. 1. They are the so-called transmission ($a$), reflection ($b$), and 90-degree ($c$) geometries. Their wave coupling characteristics are essentially different. In each case, there is a permanent pump wave and a pulse-shaped signal wave at the input. The carrier frequency of these waves is expected to be the same; in other words, we are dealing with an almost frequency-degenerate wave coupling.

For each of the schemes, we can introduce the slowly varying scalar amplitudes of the signal and pump waves, $A = A(\mathbf{r}, t)$ and $A_p = A_p(\mathbf{r}, t)$, respectively. These amplitudes are coupled via diffraction from the light-induced refractive index grating whose grating vector $\mathbf{K} = \mathbf{k} - \mathbf{k}_p$ is the difference of the corresponding light wave vectors. Because the carrier frequency for the light waves is the same, the index grating is quasistatic. The diffraction equations, which can be easily derived from the Maxwell equations, are given by [19, 20]

$$\begin{aligned} \left(\mathbf{n}\cdot\boldsymbol{\nabla} + \frac{\alpha}{2}\right) A &= -i\frac{\pi n_0^3 r}{\lambda} E_K\, A_p, \\ \left(\mathbf{n}_p\cdot\boldsymbol{\nabla} + \frac{\alpha}{2}\right) A_p &= -i\frac{\pi n_0^3 r}{\lambda}\, E_K^*\, A, \end{aligned} \tag{1}$$

where $\mathbf{n} = \mathbf{k}/k$ and $\mathbf{n}_p = \mathbf{k}_p/k_p$ are unit vectors, $\alpha$ is the light absorption coefficient, $E_K$ is the amplitude of light-induced field (the grating amplitude), $n_0$ is the background refractive index, $\lambda$ is the vacuum wavelength, and $r$ is the relevant electro-optic coefficient. The time derivatives are omitted in Eqs. (1) because light is expected to follow the refractive index changes adiabatically. The coupled-wave equations can be applied to a wide range of light-diffraction phenomena [18, 19]. In particular, they are applicable to the description of diffraction with and without change of the polarization state in anisotropic crystals [20]. Set (1) also allows important generalizations to the case of a vector wave coupling in cubic PR crystals [21]. For the geometries in Fig. 1, the operator $\mathbf{n}\cdot\boldsymbol{\nabla}$ in Eq. (1) simplifies to $\partial/\partial z$, where $z$ is the propagation coordinate.

To obtain the complete set of nonlinear equations, we need to express the grating amplitude $E_K$ in terms of the light amplitudes $A$ and $A_p$. The simplest and highly useful version of such a material equation is [18, 19]

$$\left(t_r\,\frac{\partial}{\partial t} + 1\right) E_K = \frac{E_s\, A\, A_p^*}{|A|^2 + |A_p|^2}\,, \tag{2}$$

where $t_r$ is the response time and $E_s$ is a characteristic

electric field. This equation is applicable to the cases where the restriction to a single type of charge carriers is possible. The combination of light amplitudes in the right-hand side is nothing else than the half-contrast of the light interference pattern; it determines the steady-state value of $E_K$. This distinctive feature of the PR response originates from the balance of different contributions to the electric photo-current density; the dark charge transport is thus negligible. For the same reason, the rate of relaxation of the space-charge field, $t_r^{-1}$, is proportional to the total light intensity $|A|^2 + |A_p|^2$. The response time $t_r$ can usually be identified with the dielectric relaxation time and expressed in terms of the static dielectric constant and the total photo-conductivity. It typically ranges from $10^{-3}$ to $10^2$ s in continuous-wave PR experiments.

In the case of dominating diffusion charge transport, we have $E_s = iE_D$, where $E_D = Kk_BT/e$ is the so-called diffusion field, $T$ is the absolute temperature, $k_B$ is the Boltzmann constant, and $e$ is the elementary charge. The presence of the imaginary unit $i$ implies that the index distribution is shifted by $\pi/2$ with respect to the light interference pattern. Usually, $E_D \sim 10^3$ V/cm in PR experiments. In the case of a dominating drift or photogalvanic charge transport, $E_s$ is a real quantity [19, 22]. It is equal to the applied field $E_0$ or the photogalvanic field $E_{pv}$. The latter can be as high as $10^4$–$10^5$ V/cm in $LiNbO_3$ and $LiTaO_3$ crystals. Applied electric fields can also be of this level. The index grating is unshifted (or $\pi$-shifted) in the drift-photovoltaic case. The effects of spatial dispersion can renormalize the above characteristic fields for sufficiently large values of the spatial frequency $K$ [18, 19].

Often, the light absorption is negligible for the PR effects, and we can therefore set $\alpha = 0$. In this case, as follows from Eqs. (1), we have

$$\boldsymbol{\nabla} \cdot (\mathbf{n}_p|A_p|^2 + \mathbf{n}|A|^2) = 0;$$

this relation expresses the energy conservation law during the interaction of light waves. In the important particular cases of the transmission and reflection geometries (see Fig. 1), when the light amplitudes depend only on a single propagation coordinate $z$, the energy conservation law respectively becomes $|A_p(z)|^2 + |A(z)|^2 = \text{const}$ and $|A_p(z)|^2 - |A(z)|^2 = \text{const}$.

The so-called undepleted pump approximation is used in what follows. It is applicable for sufficiently small values of the input amplitude $A(0,t)$ when $|A|^2 \ll |A_p|^2$ inside the crystal. By setting $\alpha = 0$ and $\mathbf{n} \cdot \boldsymbol{\nabla} = \partial/\partial z$, we obtain the set of coupled linear equations for the dimensionless ratios $a = A/A_p$ and $u = E_K/E_s$:

$$\frac{\partial a}{\partial z} = \gamma_0\, u, \tag{3}$$

$$\left(t_r \frac{\partial}{\partial t} + 1\right) u = a, \tag{4}$$

where the combination

$$\gamma_0 = -i\,\pi n_0^3 r\, E_s/\lambda \tag{5}$$

is the so-called coupling coefficient. It is generally a complex quantity that characterizes the type and strength of the PR response.

Using the temporal Fourier transformation $a(t) \to a_\omega$, we obtain an explicit expression for the output ratio $a_\omega(d)$ as

$$a_\omega(d) = a_\omega(0) \exp \frac{\gamma_0 d}{1 - i\omega t_r}, \tag{6}$$

where $d$ is the propagation distance for the signal wave and $a_\omega(0)$ is the input value of $a_\omega(z)$. This expression is applicable to all optical configurations in Fig. 1 within the undepleted pump approximation.

The complex function $g_\omega = \gamma_0/(1 - i\omega t_r)$ is apparently the rate of spatial changes for the $\omega$-component of the input signal. Its real part $g'_\omega$ is the rate of spatial amplification and the imaginary part $g''_\omega$ must be treated as the nonlinear correction to the wave vector component $k_z$. It is essential that the dependence $g_\omega$ is typically resonant; for $|\omega| \gg t_r^{-1}$, the rate coefficient is very small. The response time $t_r$ determines the resonance width.

Using Eq. (6), we can analyze the shape of the output pulse for different types of the PR response, different geometries, and different input signals. It is essential that the product $\gamma_0 d$ enters the exponent in the right-hand side; for $|\gamma_0|d \gg 1$, we can expect very sharp spectral dependences of the exponent and a strong impact of the type and strength of the PR response on the output pulse characteristics.

The Gaussian shape of the input signal is useful for both analytic and numerical treatments. In this case, we use the parameterization

$$A(0,t) = A_0 \exp(-t^2/t_0^2),$$

where $A_0$ is the input signal amplitude and $t_0$ is the input width parameter. Correspondingly, we have

$$A_\omega(0) = \frac{t_0}{2\sqrt{\pi}} A_0 \exp\left(-\frac{\omega^2 t_0^2}{4}\right),$$

and hence the normalized output signal $A(d,t)/A_0$ is given by

$$\frac{A(d,t)}{A_0} = \frac{t_0}{2\sqrt{\pi}} \times \times \int_{-\infty}^{\infty} \exp\left(\frac{\gamma_0 d}{1-i\omega t_r} - \frac{\omega^2 t_0^2}{4} - i\omega t\right) d\omega. \quad (7)$$

This integral cannot be calculated analytically.

Usually, the output intensity of the signal wave $I(d,t) = |A(d,t)|^2$ normalized to $I_0 = |A_0|^2$ is of main interest. In accordance with Eq. (7), we can expect both spatial amplification and phase changes to contribute to the shape of $I(d,t)/I_0$ in general.

### 3. DIFFUSION RESPONSE

This type of the PR response, which is distinguished by a real coupling constant $\gamma_0 = \pi n_0^3 r E_D/\lambda$, is the simplest. Lines *1* and *2* in Fig. 2*a* show the spectral dependence of the real and imaginary parts of the rate coefficient $g_\omega$. The amplification coefficient $g'_\omega$ is here an even function that peaks at $\omega = 0$, whereas the wave vector correction $g''_\omega$ is an odd function of the frequency $\omega$. This function is sometimes attributed to the effective group velocity $v_g(\omega) = d\omega/dg''_\omega$, which is an even function of $\omega$.

Generally, both the amplitude and phase changes, which are respectively related to $g'_\omega$ and $g''_\omega$, contribute to the output amplitude $A(d,t)$. Equation (7) then takes the form

$$\frac{A(d,t)}{A_0} = \frac{t_0}{\sqrt{\pi} t_r} \int_0^{\infty} \exp\left[\frac{\gamma_0 d}{1+s^2} - \frac{s^2 t_0^2}{4t_r^2}\right] \times \times \cos\left[s\left(\frac{t}{t_r} - \frac{\gamma_0 d}{1+s^2}\right)\right] ds \quad (8)$$

and the ratio $A(d,t)/A_0$ remains real. The shape of the output signal depends on the normalized time $t/t_r$; this dependence is controlled by two dimensionless parameters, the coupling strength $\gamma_0 d$ and the ratio $t_0/t_r$.

Line *1* in Fig. 3 is the normalized input intensity profile $I(0,t)/I_{max}(0,t)$ for $t_0/t_r = 4$, $\gamma_0 d = 0$, and lines *2*, *3*, and *4* show the normalized output intensity of the pulse $I(d,t)/I_{max}(d,t)$ for $\gamma_0 d = 3$, 6, and 9, respectively. The light absorption is neglected, which is justified for $\alpha d \ll 1$ (an easily attainable situation). We see that the output pulse maximum is essentially delayed, and the delay time $\Delta t$ increases almost linearly with increasing the coupling strength $\gamma_0 d$. Furthermore, the output pulses show a noticeable nonlinear

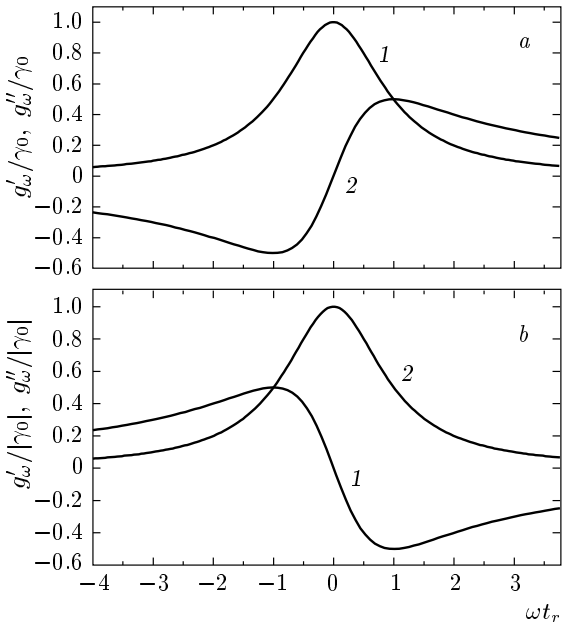


**Fig. 2.** Spectral dependences of $g'_\omega$ (curve *1*) and $g''_\omega$ (curve *2*) for the diffusion (*a*) and drift-photovoltaic (*b*) types of the PR response

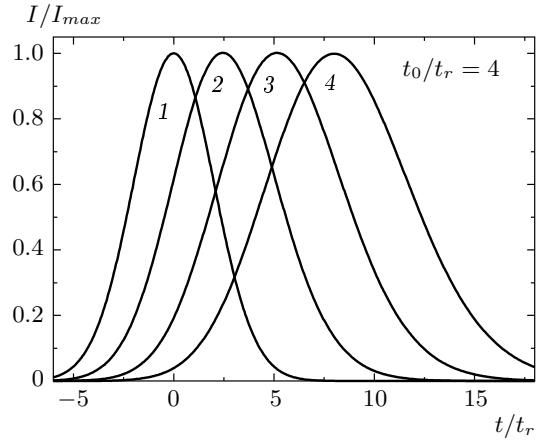


**Fig. 3.** The shape of the output signal for $t_0/t_r = 4$ and $\gamma_0 d = 0$ (*1*), 3 (*2*), 6 (*3*), and 9 (*4*); the corresponding peak amplification factors for the signal intensity are approximately 1, 243, $6.7 \cdot 10^4$, and $2.1 \cdot 10^7$

broadening; the output width is an increasing function of $\gamma_0 d$. Finally, the output pulse experiences strong spatial amplification. The peak amplification factors for $\gamma_0 d = 3$, 6, and 9 are approximately 243, $6.7 \cdot 10^4$, and $2.1 \cdot 10^7$, respectively.

Achievement of large delay times in combination with modest broadening is important for applications. In other words, the ratio of the delay time $\Delta t$ to the

half-width of the output pulse $w$ is an important figure of merit to judge about the quality of light deceleration. Furthermore, using large amplification factors is potentially dangerous because of the possibility of nonlinear losses and noise in the form of light-induced scattering [19, 20]. Therefore, it is important to investigate the key output parameters — the normalized delay time $\Delta t/t_r$, the normalized output half-width $w/t_r$, and the peak amplification factor $I(d,t)/I_{max}(d,t)$ — as functions of the input parameters $\gamma_0 d$ and $t_0/t_r$.

Using the saddle-point method [23], it is not difficult to obtain the approximate relations

$$\frac{\Delta t}{t_r} \approx \gamma_0 d, \quad \frac{w}{t_r} \approx \sqrt{2\ln 2\,\gamma_0 d + w_0^2/t_r^2} \qquad (9)$$

from Eq. (8), where $w_0 = \sqrt{\ln 2/2}\ t_0 \approx 0.6 t_0$ is the input half-width of the pulse. Equations (9) are applicable for $\gamma_0 d \gg 1$. In accordance with the data in Fig. 3, the normalized delay time increases linearly with $\gamma_0 d$ and is furthermore independent of $t_0/t_r$. Behavior of the output half-width is different. The nonlinear broadening is small for $\gamma_0 d \ll t_0^2/t_d^2$ and is proportional to $(\gamma_0 d)^{1/2}$ in the opposite limit. Within the range of parameters $t_0/t_r \ll \gamma_0 d \ll t_0^2/t_r^2$, we simultaneously have $\Delta t \gg w$ and $w \approx w_0$. This range is apparently the most profitable for the deceleration purposes. To fulfill the necessary requirements, we have to use sufficiently broad input pulses and quite large values of the coupling strength.

The solid lines in Fig. 4 show the dependences of $\Delta t/t_r$, $w/t_r$, and $I_{max}/I_0$ on the ratio $t_0/t_r$ for several representative values of $\gamma_0 d$; these lines are obtained numerically from Eq. (8) without any approximations. The normalized delay time $\Delta t/t_r$ increases rather slowly with increasing $t_0/t_r$ and is given by Eq. (9) with a good accuracy. The exact and approximate dependences $w/t_r(t_0/t_r)$ (with the latter shown by dashed lines) are already close to each other for moderate values of the coupling strength. For sufficiently large values of $t_0/t_r$, we have $w \approx w_0$. For not very narrow input pulses, the amplification factor $I_{max}/I_0$ is a slowly increasing function of $t_0/t_r$ (see Fig. 4*c*). For $t_0/t_r \gtrsim (\gamma_0 d)^{1/2}$, it is not far from the value $\exp(2\gamma_0 d)$, which corresponds to the steady-state continuous-wave spatial amplification.

The data in Fig. 4 allow optimizing the input parameters depending on the chosen figures of merit for the output characteristics. If maximizing the ratio $\Delta t/w$ is the main goal, the ratio $t_0/t_r$ can be chosen quite small; this additionally allows avoiding large amplification factors. If the goal is to maximize $\Delta t$ and avoid strong broadening, then the maximum available

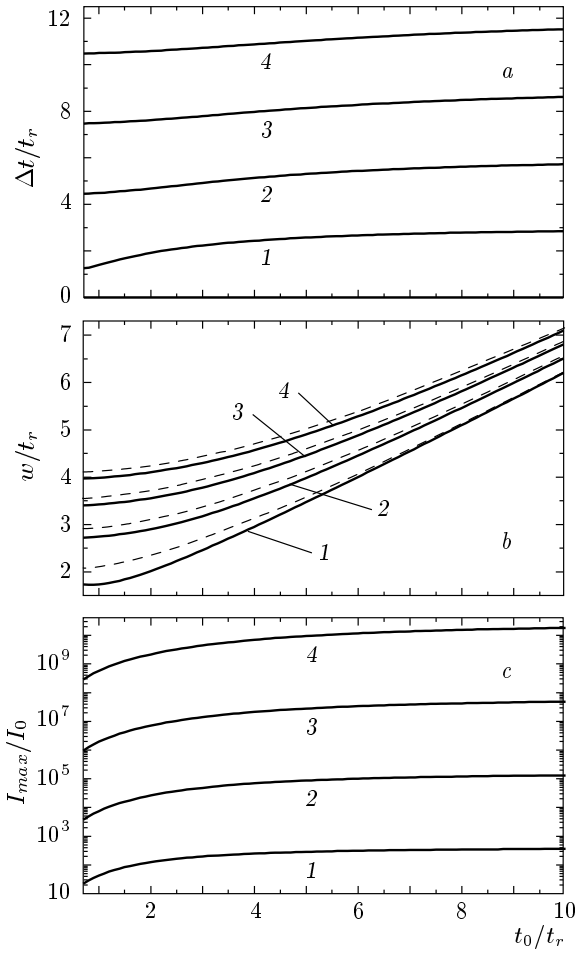


**Fig. 4.** The ratios $\Delta t/t_r$ (*a*), $w/t_r$ (*b*), and $I_{max}(d,t)/I_0$ (*c*) versus the normalized input width parameter $t_0/t_r$; $\gamma_0 d = 3$ (*1*), 6 (*2*), 9 (*3*), 12 (*4*). The dashed lines in subfigure *b* correspond to Eq. (9)

values of $\gamma_0 d$ and sufficiently large values of $t_0/t_r$ are needed; the amplification factor can be very large in this case.

The ratio $v = d/\Delta t$ can be treated as the pulse velocity. For $\Delta t/t_r \approx \gamma_0 d$, we have $v \approx 1/\gamma_0 t_r$. The nonlinear origin of this relation is evident. The larger the coupling coefficient $\gamma_0$, the smaller is $v$. Because $t_r \propto 1/I_p$, the pulse velocity increases linearly with increasing the pump intensity $I_p$. It ranges roughly from $10^{-2}$ to $10^4$ cm/s in PR experiments with continuous-wave lasers.

It is of general interest to qualitatively explain the strong effect of light deceleration. We consider what happens to the pulse during its passage through the sample in the presence of a pump. The leading edge travels almost freely because the index grating is very weak and the pump wave cannot yet feed the signal.

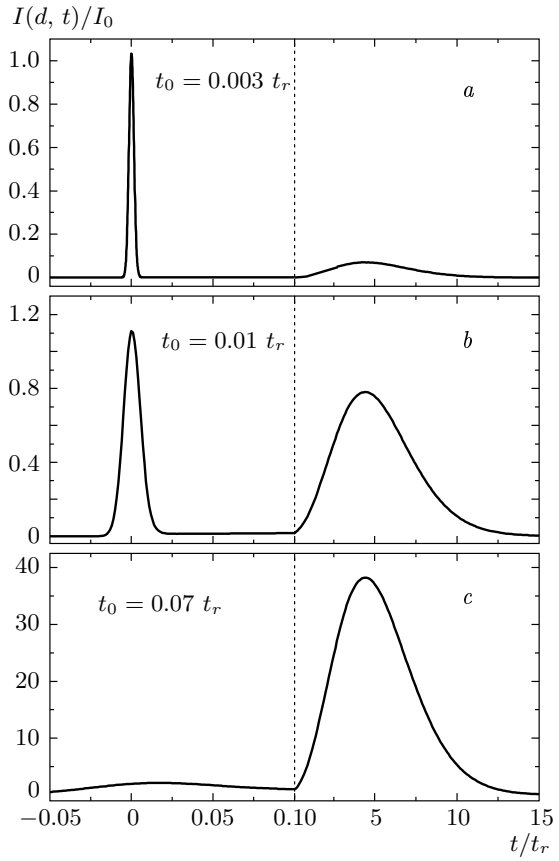


**Fig. 5.** Two-peak dynamics for narrow input pulses at $\gamma_0 d = 6$; $t_0/t_r = 0.003$ ($a$), 0.01 ($b$), and 0.07 ($c$). Note different scales for $t/t_r < 0.1$ and $> 0.1$

With time passing, the grating becomes stronger and the output pulse experiences progressing amplification via diffraction of the pump wave. Even more importantly, the grating buildup persists for a sufficiently long time after the input signal has passed its maximum and decreased considerably. This persisting grating recording is of a purely nonlinear nature: the light contrast remains high in the depths of the crystal because of strong diffraction of a weak signal at large values of $\gamma_0 d$. This effect is known since the 1980s as "self-enhancement" of the photorefractive two-wave coupling [19], but it was not considered in the context of pulse propagation. In our case, the output pulse maximum is essentially delayed because of this effect compared to that of the input signal. The thicker the sample, the longer is the delay time.

We have considered the nonlinear pulse propagation for sufficiently large values of the input half-width, $t_0/t_r \gtrsim 1$. New qualitative features appear for $t_0/t_r \ll 1$. These features are illustrated in Fig. 5 for $\gamma_0 d = 6$. At $t_0/t_r = 0.003$, the output signal consists of a pronounced very narrow nonshifted peak and a weak and broad delayed peak (see Fig. 5$a$), with the peak situated at $t/t_r \approx \gamma_0 d$. With increasing $t_0/t_r$, the shifted peak rapidly increases, while the unshifted peak experiences broadening and becomes a secondary feature (Fig. 5$b$). For $t_0/t_r \gtrsim 0.07$, the narrow peak disappears in a threshold manner and we return to the single-peak behavior (see Fig. 5$c$). The smaller $\gamma_0 d$, the larger is the critical value of $t_0/t_r$.

We now turn to analogies between the light deceleration characteristics in the PR and EIT cases. These analogies are restricted to the case of the diffusion PR response. In the EIT case, the half-value of the absorption coefficient $\alpha/2$ plays the role of the coupling constant $\gamma_0$, and the resonant nonlinearity makes the medium transparent. To obtain the simplest dynamic equations of the EIT technique, we must treat $u$ and $t_r$ as the degree and rise time of atomic coherence in Eq. (4) and then replace Eq. (3) for $a$ with

$$\left(\frac{\partial}{\partial z} + \frac{\alpha}{2}\right) a = \frac{\alpha}{2}\, u. \tag{10}$$

If $I(t/t_r, \gamma_0 d, t_0/t_r)/I_0$ describes the normalized output intensity profile calculated from Eq. (8), then the function

$$\exp(-\alpha d)\, I(t/t_r, \alpha d/2, t_0/t_r)/I_0$$

describes this profile in the EIT case. In other words, we have an additional amplification factor $\exp(2\gamma_0 d)$ in the PR case; for moderate values of the coupling strength $\gamma_0 d \lesssim 10$, this can be considered a positive factor. The shape characteristics $\Delta t/t_r$ and $w/t_r$ are the same for $\alpha = 2\gamma_0$.

It is essential that the product $\alpha d$ reaches the value of approximately 70 in the EIT experiments [2]. In the PR case, to achieve the $\Delta t/t_r$ and $w/t_r$ values comparable with those in the EIT case, we must use $\gamma_0 d \approx 35$. These high values of the coupling strength can hardly be realistic because of strong parasitic light-induced scattering that originates from spatial amplification of the weak seed scattering [19, 20].

At first sight, the analogy between the PR and EIT cases becomes complete and the restrictions from above on $\gamma_0 d$ become lifted if we use a sufficiently large light absorption in the PR case, such that $\alpha = 2\gamma_0$. Technically, this is possible because the wavelength $\lambda$ can be chosen to be close to the fundamental absorption edge. But this idea does not work for the most common transmission and reflection configurations (see Figs. 1$a$,$b$). The point is that the pump amplitude $A_p$ decays with the rate $2\gamma_0$ in this case (see Eqs. (1)), and hence the

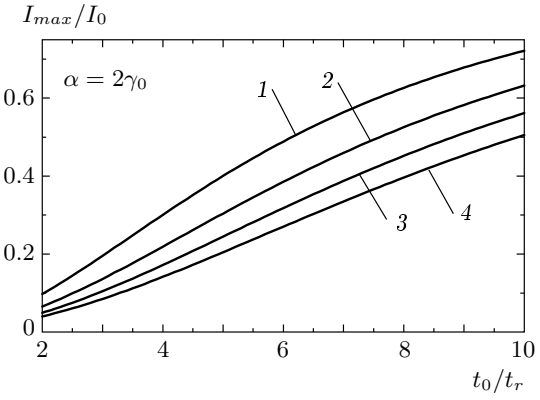


**Fig. 6.** The amplification factor $I_{max}(d,t)/I_0$ versus $t_0/t_r$ for $\alpha = 2\gamma_0$; $\gamma_0 d = 10$ (*1*), 15 (*2*), 20 (*3*), 25 (*4*)

undepleted pump approximation fails. However, it can be implemented in the 90° configuration depicted in Fig. 1*c*. In this case, the propagation distances can be made strongly different for the pump and signal waves. When the propagation distance for the pump wave is considerably shorter than $1/2\gamma_0$, the undepleted pump approximation can be used again such that the complete analogy with the EIT case is maintained. It is indeed necessary to add the term $\alpha a/2$ to the left-hand side of Eq. (3). We finally note that the 90° geometry is expected to be very useful for light deceleration in waveguides pumped through the surface.

Figure 6 shows the expected dependence $I_{max}/I_0$ on $t_0/t_r$ in the 90° geometry for several representative large values of the coupling strength and $\alpha = 2\gamma_0$. We see that the output pulse is moderately attenuated. Good shape characteristics are ensured in accordance with Eq. (9). Generally speaking, it is possible to achieve the same input and output peak intensities of the pulse by properly adjusting the absorption coefficient $\alpha$.

Finally, we note the following. It is known that the value of $\gamma_0$ as a function of the spatial frequency $K$ has a maximum at $KR_D \approx 1$, where $R_D$ is the Debye screening length determined by the effective trap concentration [18, 19]; it is often comparable to the light wavelength $\lambda$. To minimize the negative influence of the light-induced scattering for large values of the coupling strength, it is expedient to use experimental configurations with $K \approx R_D^{-1}$; the use of the diffusion-driven PR nonlinearity is optimum in this case. Another possibility is the use of the reflection geometry (see Fig. 1*b*) and narrow counter-propagating pump and signal beams. The wide-angle light-induced scattering is then suppressed for geometric reasons.

## 4. DRIFT-PHOTOVOLTAIC RESPONSE

In this case, the coupling constant is purely imaginary and can be presented as $\gamma_0 = -i|\gamma_0|$ without loss of generality. In contrast to the diffusion case, the amplification coefficient $g'_\omega$ and the wave-vector correction $g''_\omega$ are odd and even functions of $\omega$, respectively (see Fig. 2*b*), and the steady-state ($\omega = 0$) amplification of the signal wave is absent. The effective group velocity $v_g = d\omega/dg'_\omega$ is an odd function of $\omega$. We note that the attainable values of $|\gamma_0|$ are generally larger than the values of $\gamma_0$ in the diffusion case because the applied (or photovoltaic) field can be made larger than the diffusion field $E_D$.

Both phase and amplitude changes again contribute to the output amplitude $A(d,t)$, but the ratio $A(d,t)/A_0$ is essentially complex now. With Eq. (7), it can be represented as

$$\frac{A(d,t)}{A_0} = \frac{t_0}{\sqrt{\pi}\, t_r} \int\limits_0^\infty \exp\left(-\frac{s^2 t_0^2}{4t_r^2}\right) (F'_s - iF''_s)\, ds, \quad (11)$$

where the functions $F'_s$ and $F''_s$ are given by

$$\begin{aligned} F'_s &= \cos\frac{|\gamma_0|d}{1+s^2}\,\mathrm{ch}\,\frac{s|\gamma_0|d}{1+s^2}\cos(st) - \\ &\quad - \sin\frac{|\gamma_0|d}{1+s^2}\,\mathrm{sh}\,\frac{s|\gamma_0|d}{1+s^2}\sin(st), \\ F''_s &= \cos\frac{|\gamma_0|d}{1+s^2}\,\mathrm{sh}\,\frac{s|\gamma_0|d}{1+s^2}\sin(st) + \\ &\quad + \sin\frac{|\gamma_0|d}{1+s^2}\,\mathrm{ch}\,\frac{s|\gamma_0|d}{1+s^2}\cos(st). \end{aligned} \quad (12)$$

The shape of the output signal is again controlled by two dimensionless parameters $t_0/t_r$ and $|\gamma_0|d$.

Figure 7 gives representative examples for the time dependence of the normalized output intensity $I(d,t)/I_0$. Qualitatively, the situation looks similar to that in the diffusion case, see Fig. 3. We have a pronounced time shift $\Delta t$, which increases practically linearly with increasing the coupling strength $|\gamma_0|d$, and a noticeable broadening. At the same time, the peak amplification factors are considerably smaller than earlier (cf. Fig. 3) despite larger values of the coupling strength. We also note that a smooth bell-shape output profile $I(d,t)$ is now a superposition of strongly modulated components $|A'(d,t)|^2$ and $|A''(d,t)|^2$; this modulation can be attributed to the pump-induced nonlinear frequency shift for the signal wave.

We now consider the dependences of the key output parameters of the pulse on the key input parameters. Figure 8 shows the ratios $\Delta t/t_r$, $w/t_r$, and $I_{max}/I_0$

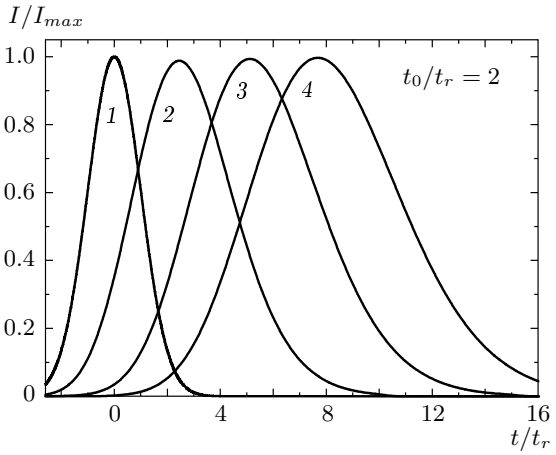


**Fig. 7.** The normalized output intensity versus the normalized time for $t_0/t_r = 2$ and $|\gamma_0|d = 0$ (the input profile) (*1*), 5 (*2*), 10 (*3*), 15 (*4*). The peak amplification factors are $I_{max}/I_0 \approx 11.8$ (*2*), $8.9 \cdot 10^2$ (*3*), $8.8 \cdot 10^4$ (*4*)

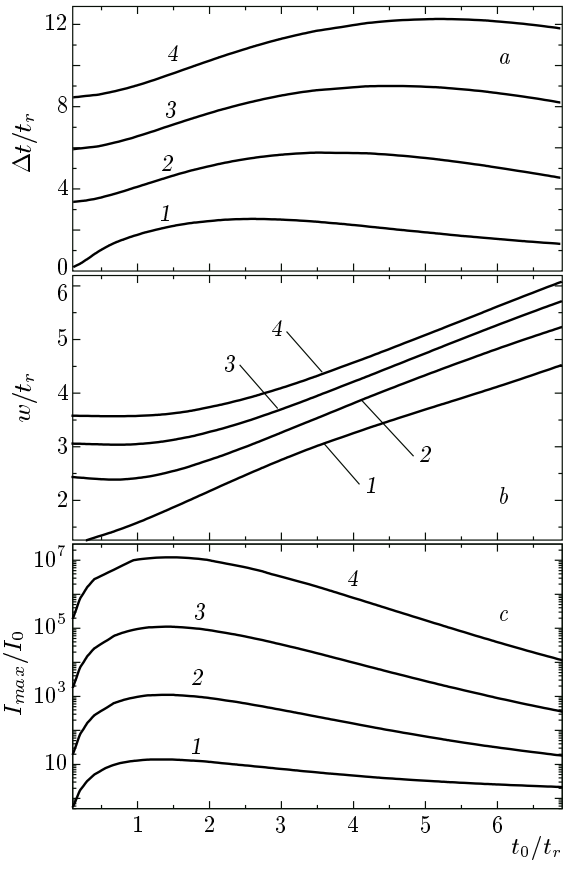


**Fig. 8.** Dependences of $\Delta t/t_r$, $w/t_r$, and $I_{max}/I_0$ on $t_0/t_r$; $|\gamma_0|d = 5$ (*1*), 10 (*2*), 15 (*3*), 20 (*4*)

as functions of $t_0/t_r$ for several representative values of the coupling strength $|\gamma_0|d$. The functional dependences differ considerably from those typical for the diffusion case (cf. Fig. 4). Furthermore, the actual values of $|\gamma_0|d$ are noticeably larger in the present case because of relatively low amplification factors and the values of $t_0/t_r$ are somewhat smaller than previously.

The normalized delay time $\Delta t/t_r$ increases, as previously, almost linearly with increasing $|\gamma_0|d$, but its dependence on the input-width parameter $t_0/t_r$ is different; it is characterized by a broad maximum, as can be seen in Fig. 8*a*. For the position of this maximum, we have $[t_0/t_r]_{max} \approx \sqrt{|\gamma_0|d}$. At the same coupling strength, the maximum value of $\Delta t/t_0$ is roughly two times smaller than in the diffusion case. This means that the pulse speed can be estimated as $v \approx 2/|\gamma_0|t_r$. The dependence of the output width parameter $w/t_r$ on $t_0/t_r$ and $|\gamma_0|d$ (see Fig. 8*b*) is qualitatively similar to that in the diffusion case. Roughly, the ratio $w/t_r$ is two times smaller than previously. We note that the ratio $\Delta t/w$ also has a maximum as a function of $t_0/t_r$. At the same coupling strength, the peak amplification factor $I_{max}/I_0$ is much smaller compared with the diffusion case. In contrast to that case, this factor has a maximum as a function of $t_0/t_r$. All the distinctive features mentioned originate from the difference in the spectral behavior of $g_\omega$. The essence of this difference is indeed the presence of the steady-state ($\omega = 0$) spatial amplification in the diffusion case and its absence in the drift-photovoltaic case.

Two variants for optimization of the deceleration characteristics can be proposed for the local response. First, quite large values of the ratio $\Delta t/w$ can be achieved for rather small $t_0/t_r$ and not very large $|\gamma_0|d$; the last condition leads to moderate amplification factors. For example, the ratio $\Delta t/w_0 \approx 2$ is obtained for $t_0/t_r = 2$ and $\gamma_0 d = 10$; for these parameters, we have $I_{max}/I_0 < 10^3$. The shape of the output pulse can be seen from Fig. 7. Second, sufficiently large values of $t_0/t_r$ and $|\gamma_0|d$ can be used. This allows avoiding too large amplification factors ($I_{max}/I_0 \lesssim 10^4$) in accordance with the data in Fig. 8 to reduce the danger coming from the light-induced scattering. The ratio $\Delta t/w$ can exceed 2 in this case.

We finally mention that the two-peak regime of nonlinear pulse propagation, which has been found in the diffusion case for very small values of the input-width parameter $t_0/t_r$ (see Fig. 5), also occurs in the drift-photovoltaic case. This regime is inherent in any type of the PR response.

### 5. DECELERATION WITH PUMP PULSES

Above, we have restricted ourselves to the case of a permanent pump wave. It is possible and important to generalize the results obtained to the case where the pump is pulsed. Equations (3) and (4) for $a = A/A_p$ and $u = E_K/E_s$, obtained within the undepleted pump approximation, are still applicable, but the response time $t_r \propto |A_p|^{-2}$ becomes time dependent. This complication can, however, be overcome by a time renormalization.

For simplicity, we let the pump intensity be a Gaussian function of time,

$$A_p = A_p^0 \exp(-t^2/t_p^2),$$

where $A_p^0$ and $t_p$ are the amplitude and the width parameter of the pump pulse. Then we can replace the time $t$ with

$$\tau = \sqrt{\pi/8}\, t_p \,\mathrm{Erf}\left(\sqrt{2}\, t/t_p\right),$$

where

$$\mathrm{Erf}(x) = \frac{2}{\sqrt{\pi}} \int\limits_0^x \exp(-s^2)\, ds$$

is the error function. After that, Eq. (4) acquires the form

$$\left(t_r^0 \frac{\partial}{\partial \tau} + 1\right) u = a, \tag{13}$$

where $t_r^0 = t_r(|A_p^0|^2)$ is the characteristic response time for the peak value of the pump intensity. The structure of this equation is identical to that of Eq. (4). Furthermore, the input values of the amplitudes $a$, $A$, and $A_p$ can be expressed in terms of $\tau$. After that, the output amplitude $A(d,t)$ can be found via the Fourier transformation. In the diffusion case, the final expression for the ratio $A(d,t)/A_0$ is

$$\frac{A(d,t)}{A_0} = \exp\left(-\frac{t^2}{t_1^2}\right) \times$$

$$\times \int\limits_{-\infty}^{\infty}\!\!\int \exp\left(\frac{\gamma_0\, d}{1+\omega^2} - \frac{t'^2 + 2tt'}{t_2^2}\right) \times$$

$$\times \cos\left[\omega\left(\frac{\gamma_0\, d}{1+\omega^2} + \tau(t')\right)\right] \frac{dt'd\omega}{2\pi}, \tag{14}$$

where

$$t_1^{-2} = 2t_p^{-2} + t_0^{-2}, \quad t_2^{-2} = t_p^{-2} + t_0^{-2},$$

and all time parameters are measured in the units of $t_r^0$.

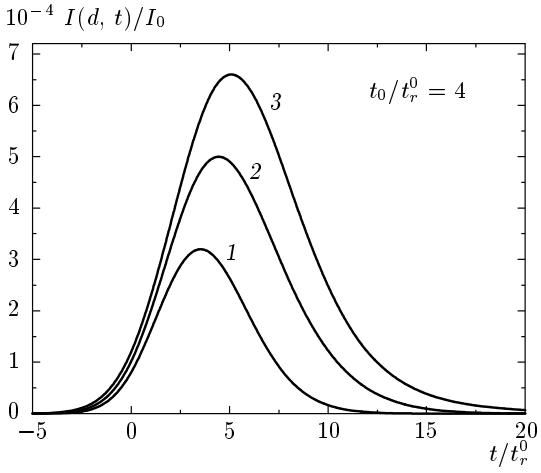


**Fig. 9.** The influence of the pump pulse duration on the deceleration characteristics for the diffusion response at $\gamma_0 d = 6$ and $t_0/t_r^0 = 4$; $t_p/t_r^0 = 7$ (*1*), 10 (*2*), 20 (*3*)

Figure 9 shows the effect of the pump pulse duration on the output profile of the signal for the diffusion response, with $\gamma_0 d = 6$ and $t_0/t_r^0 = 4$. We see that the time delay, the output width, and the maximum intensity remain weakly perturbed for $t_p/t_r^0 = 20$ (cf. Fig. 3). For smaller values of the pump-width parameter $t_p$, the changes in the output characteristics become significant. They manifest themselves in smaller time delays and amplification factors. Apparently, the pump pulse half-width has to be larger than the delay time in order to avoid strong distortions of the output signal.

### 6. DISCUSSION

Several different issues are worthy of attention.

Our results show clearly that the coupling strength $|\gamma_0|d$ is the key parameter for pulse deceleration, irrespective of the type of the PR response. For $|\gamma_0|d \lesssim 1$, we inevitably deal with the situation where the deceleration effect is small and barely distinguishable against the shape distortions and noise. The pulse velocity defined as the velocity of the pulse maximum has a conditional acceptance in this case. In short, true deceleration must be considered an essentially nonlinear phenomenon. Most probably, this assertion is applicable to any kind of nonlinear deceleration, including the EIT technique.

The necessity of a strong nonlinearity leads to two general problems: how to obtain it and what are possible negative side effects. In the photorefractive (PR) case, the attainment of large values of $|\gamma_0|d$ already

at low and/or moderate intensities is not a serious problem. Among negative consequences of a strong PR nonlinearity, the most important is probably the wide-angle light-induced scattering. Another possible drawback is the instabilities of two-wave coupling schemes. Potentially, the reflection geometry is most dangerous in this sense. Here, the instabilities often manifest themselves as threshold-type optical oscillations [19, 24]. The problem of negative nonlinear side effects should be inherent to any nonlinear deceleration method. Particularities of the nonlinear limitations can be strongly different for different schemes and techniques.

In spite of the presence of common features, the light deceleration characteristics are essentially different for the diffusion and drift-photovoltaic PR responses. Each of these cases has certain advantages and drawbacks. Importantly, the level of the nonlinear light-induced scattering is also strongly dependent on the type of the PR response. Further studies are necessary to establish the limits for the deceleration characteristics in different nonlinear schemes/materials.

In this regard, considering other important, but more special, types of the PR response could be interesting. First, this is the fast resonant response typical of cubic crystals of the sillenite family, $Bi_{12}SiO_{20}$, $Bi_{12}TiO_{20}$, and $Bi_{12}GeO_{20}$ [18, 19]. Its specific features come from both the vectorial character of the wave interaction and an almost imaginary rate constant $t_r^{-1}$ for the space-charge field [21, 25]. Second, this is the self-compensating response typical of $Sn_2P_2S_6$ crystals [26, 27]. This response involves two types of charge carriers and remains strong in the near-infrared range, which is important in applications. In both cases, the spectral dependence of the PR response is more complicated compared to the above diffusion and drift-photovoltaic responses. We can therefore expect specific features of light deceleration in these materials.

The most important advantages of the PR nonlinearity over many other known nonlinear responses are its diversity and high strength already at low light intensities, a high spectral and temperature tolerance, and the possibility to use different interaction schemes. The main drawback of the PR nonlinearity is its slowness; the response time ranges roughly from $10^2$ to $10^{-3}$ s for continuous-wave lasers. To overcome this disadvantage and obtain much shorter response times, it is necessary to switch to pulsed lasers. Conceptually, increasing light intensity up to the MW/cm$^2$ range does not change the nature of the PR nonlinearity. This should allow proceeding to the nanosecond range of the pulse duration at least. The effects of finite pump-pulse width considered briefly in Sec. 5 become indeed increasingly important in this range. For typical photorefractive parameters, the pulse velocity estimated as $v \sim (|\gamma_0| t_r)^{-1}$ can range from $\sim 10^{-4}$ to $\sim 10^6$ cm/s depending on the light intensity.

## 7. CONCLUSIONS

The photorefractive nonlinearity offers superior possibilities for deceleration of light pulses. The propagation velocity can be varied over a wide range the delay times exceeding the pulse half-width are attainable. Characteristics of light deceleration depend essentially on the type of the photorefractive response. The pulse deceleration effect is essentially nonlinear; high values of the coupling strength are needed to achieve outstanding deceleration characteristics. Despite the specificity of the photorefractive deceleration method, it shows deep analogies with the EIT-based deceleration technique.

Financial support from the Russian Foundation for Basic Research (Grant № 07-02-00301a) is gratefully acknowledged.

## REFERENCES

1. L. V. Hau, S. E. Harris, Z. Dutton, and C. Behroozi, Nature **397**, 594 (1999).
2. C. Liu, Z. Dutton, C. Behroozi, and L. V. Hau, Nature **409**, 490 (2001).
3. R. W. Boyd and D. J. Gauthier, Progr. Opt. Vol. 43, ed. by E. Wolf, Elsevier, Amsterdam (2002).
4. M. S. Bigelow, N. N. Lepeshkin, and R. W. Boyd, Science **301**, 200 (2003).
5. M. O. Scully and G. R. Welch, Phys. World, October (2004), p. 31.
6. S. E. Harris, Phys. Today **50**, 36 (1997).
7. D. F. Phillips, A. Fleischhauer, A. Mair, R. L. Walsworth, and M. D. Lukin, Phys. Rev. Lett. **86**, 783 (2001).
8. A. Turukhin, V. Sudarshanam et al., Phys. Rev. Lett. **88**, 023602 (2002).
9. M. S. Bigelow, N. N. Lepeshkin, and R. W. Boyd, Phys. Rev. Lett. **90**, 113903 (2003).
10. A. Schweinsberg, N. N. Lepeshkin, M. S. Bigelow, R. W. Boyd, and S. Jarabo, Europhys. Lett. **73**, 218 (2006).

**11**. E. B. Aleksandrov and V. S. Zapasski, Uspekhi Fiz. Nauk **174**, 1105 (2004).

**12**. M. Scully and M. Fleischhauer, Phys. Rev. Lett. **69**, 1360 (1992).

**13**. Z. Dutton and L. V. Hau, Phys. Rev. A **70**, 053831 (2004).

**14**. E. Podivilov, B. Sturman, A. Shumelyuk, and S. Odoulov, Phys. Rev. Lett. **91**, 083902 (2003).

**15**. A. Shumelyuk, K. Shcherbin, S. Odoulov, B. Sturman, E. Podivilov, and K. Buse, Phys. Rev. Lett. **93**, 243604 (2004).

**16**. G. Zhang, R. Dong, F. Bo, and J. Xu, Appl. Opt. **43**, 1167 (2004).

**17**. G. Zhang, F. Bo, R. Dong, and J. Xu, Phys. Rev. Lett. **93**, 133903 (2004).

**18**. M. P. Petrov, S. I. Stepanov, and A. V. Khomenko, *Fotorefraktivnye kristally v kogerentnoy optike*, Nauka, Sankt-Peterburg (1992) [M. P. Petrov, S. I. Stepanov, and A. V. Khomenko, *Photorefractive Crystals in Coherent Systems*, Springer-Verlag, Berlin (1992)].

**19**. L. Solymar, D. Webb, and A. Grunnet-Jepsen, *The Physics and Applications of Photorefractive Materials*, Clarendon Press, Oxford (1996).

**20**. B. I. Sturman, S. G. Odoulov, and M. Yu. Goulkov, Phys. Rep. **275**, 199 (1996).

**21**. B. I. Sturman, E. V. Podivilov, K. H. Ringhofer, E. Shamonina, V. P. Kamenov, E. Nippolainen, V. V. Prokofiev, and A. A. Kamshilin, Zh. Eksp. Teor. Fiz. **119**, 125 (2001).

**22**. B. I. Sturman and V. M. Fridkin, *Fotogal'vanicheskij effekt v sredax bez centra simmetrii i rodstvennye yavleniya*, Nauka, Moskva (1992) [B. I. Sturman and V. M. Fridkin, *The Photovoltaic and Photorefractive Effects in Noncentrosymmetric Crystals*, Gordon and Breach, Philadelphia (1992)].

**23**. J. Mathews and R. L. Walker, *Mathematical Methods of Physics*, Benjamin, New York (1964).

**24**. S. G. Odoulov, M. S. Soskin, and A. I. Khiznyak, *Lazery na dinamicheskikh reshetkakh*, Nauka, Moskva (1990) [S. G. Odoulov, M. S. Soskin, and A. I. Khiznyak, *Dynamic Grating Lasers*, Harwood, London (1991)].

**25**. B. I. Sturman, in *Photorefractive Materials and Their Applications*, Vol. 1, ed. by P. Günter and J. Huignard, Springer-Verlag, New York (2006), p. 119.

**26**. S. G. Odoulov, A. N. Shumelyuk, U. Hellwig, R. A. Rupp, A. A. Grabar, and I. M. Stoika, J. Opt. Soc. Amer. B **13**, 2352 (1996).

**27**. A. A. Grabar, Yu. M. Vysochanskii, A. N. Shumelyuk, M. Jazbinsek, G. Montemezzani, and P. Günter, in *Photorefractive Materials and Their Applications*, Vol. 2, ed. by P. Günter and J.-P. Huignard, Springer-Verlag, New York (2006), p. 327.